J|A|C|S
ARTICLES

Published on Web 10/25/2008

Diastereoselective Addition of Zincated Hydrazones to Alkenylboronates and Stereospecific Trapping of Boron/Zinc Bimetallic Intermediates by Carbon Electrophiles

Takuji Hatakeyama,† Masaharu Nakamura,† and Eiichi Nakamura*

Department of Chemistry, The University of Tokyo, Hongo, Bunkyo-ku, Tokyo 113-0033, Japan

Received August 9, 2008; E-mail: nakamura@chem.s.u-tokyo.ac.jp

Abstract: Zincated hydrazones possessing a *tert*-butyl group on the zinc atom undergo addition to (*E*)- or (*Z*)-alkenylboronic acid pinacol esters to produce α-alkylated-γ-boryl-γ-zinciohydrazone intermediates with good to excellent diastereoselectivity (*ds*). The 1,1-organodimetallic intermediate possessing a boron atom and a zinc atom in the position γ to the hydrazone group undergoes further C−C bond formation with a carbon electrophile to give a γ-boryl hydrazone possessing several contiguous stereogenic centers with up to 99% *ds*. The (*S*)-1-amino-2-methoxymethylpyrrolidine hydrazone shows a high level of asymmetric induction in the addition/trapping sequence. Density functional theory calculations on the pathways of the addition reaction revealed a metallo-ene mechanism consisting of the formation of a π complex between a zincated hydrazone and a vinylborane followed by a six-centered bond reorganization of a highly ordered boat conformation transition state. The calculations indicated that the use of the zinc atom together with the imine or hydrazone is the key for the success of the olefinic variant of the aldol reaction that has long been considered not to take place because of the endothermicity of the reaction and has never been examined with any seriousness by chemists. The steric repulsion caused by the bulky *tert*-butyl ligand on the zinc atom and the pinacol moiety of the vinylboronate substrates in the highly ordered transition structures gives rise to the observed high *ds* of the present carbozincation reaction.

Introduction

Stereocontrol in the construction of multiple stereogenic centers has been a central issue of organic synthesis for a long time, and those in acyclic systems remain a challenge. We considered over a decade ago that the addition of a metal enolate to an unactivated olefin might be a potentially powerful method to achieve stereocontrol of multiple stereogenic centers during formation of new C−C bonds (Scheme 1, middle). The γ-metalated carbonyl or imine compounds are the homologues of metal enolates[1] and metal homoenolates (β-metalated carbonyl compounds),[2,3] in which we have had a longstanding interest. Such a reaction, however, did not exist in the literature. In fact, quantum-mechanical calculations of any kind would indicate that the addition of the enolate anion of acetone to ethylene is highly endothermic and will hardly take place. This reaction is electronically equivalent to the aldol reaction that has long served as a prototype of acyclic stereocontrol (Scheme 1, top). The olefinic variant (Scheme 1, middle), however, is potentially much more interesting in that one can use the initial addition product for possible further C−C bond formation. It should be noted that such reactions are different both mechanistically and synthetically from Michael addition reactions.

Scheme 1. Addition of Metal Enolates to Carbonyls and Olefins

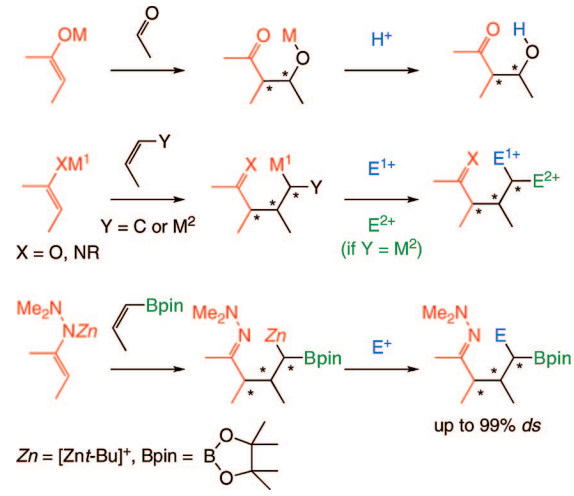

The initial success of our exploration was limited to a strained olefin[4] and intermolecular cyclization,[5] but we quickly discovered that these limitations can readily be removed. Thus, we

† Present address: International Research Center for Elements Science, Institute for Chemical Research, Kyoto University, Uji, Kyoto 611-0011, Japan.

(1) Kuwajima, I.; Nakamura, E. *Acc. Chem. Res.* **1985**, *18*, 181–187.
(2) (a) Kuwajima, I.; Nakamura, E. *J. Am. Chem. Soc.* **1977**, *99*, 7360–7361. (b) Nakamura, E.; Kuwajima, I. *J. Am. Chem. Soc.* **1983**, *105*, 651–652. (c) Aoki, S.; Fujimura, T.; Nakamura, E.; Kuwajima, I. *J. Am. Chem. Soc.* **1988**, *110*, 3296–3298.
(3) Nakamura, E.; Kuwajima, I. *J. Am. Chem. Soc.* **1984**, *106*, 3368–3370.
(4) Nakamura, E.; Kubota, K. *J. Org. Chem.* **1997**, *62*, 792–793.
(5) (a) Nakamura, E.; Sakata, G.; Kubota, K. *Tetrahedron Lett.* **1998**, *39*, 2157–2158. (b) Lorthiois, E.; Marek, I.; Normant, J. F. *J. Org. Chem.* **1998**, *63*, 2442–2450. (c) Karoyan, P.; Chassaing, G. *Tetrahedron Lett.* **1997**, *38*, 85–88.

10.1021/ja806258v CCC: $40.75

Scheme 2. Stereocontrolled Construction of Multiple Stereogenic Centers by an Addition/Trapping Sequence

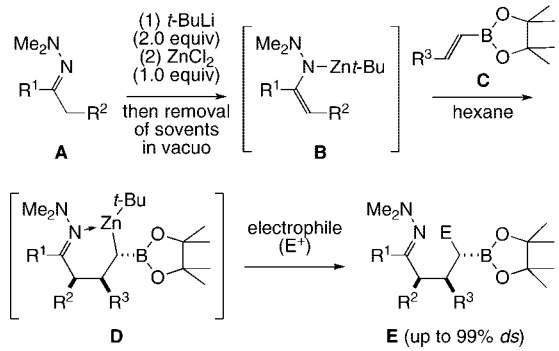

Scheme 3. Addition of a Zincated Hydrazone Possessing an Alkyl Dummy Ligand to (*E*)- or (*Z*)-Hexenylboronate

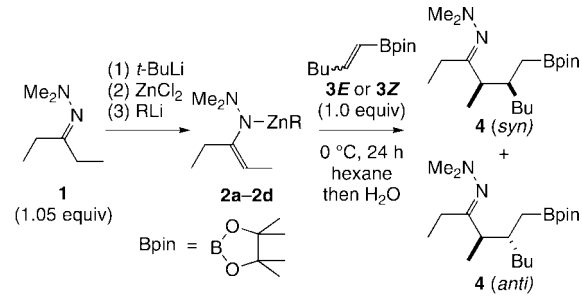

Table 1. Effect of Dummy Ligands on *ds* and Reactivity

entry	hexenylboronate[a]	R, **2a–2d**	*syn*:*anti*[b]	yield
1		*t*-Bu, **2a**	95.2:4.8	88%[c]
2	Bu–⁄⁄–Bpin	*sec*-Bu, **2b**	45.0:55.0	69%[d]
3		Bu, **2c**	32.9:67.1	60%[d]
4	**3*E*** (99.7%*E*)	Cl, **2d**[e]	—	0%[d]
5		*t*-Bu, **2a**	25.6:74.4	80%[c]
6	Bpin–⁄⁄–Bu	*sec*-Bu, **2b**	33.8:66.2	84%[d]
7	**3*Z*** (99.0%*Z*)	Bu, **2c**	28.0:72.0	66%[d]

[a] Bpin = 4,4,5,5-tetramethyl-1,3,2-dioxaborolanyl. [b] Diastereoselectivities were determined by GC analyses of the crude product. [c] Isolated yield. [d] Yield was determined by ^{1}H NMR spectroscopy. [e] Zincated hydrazone **2d** was prepared via two steps: (1) deprotonation with *t*-BuLi and (2) transmetalation with $ZnCl_2$.

discovered that zincated hydrazones and imines [M^1 = Zn(II)] readily add to ethylene[6] (Y = H) and vinylmagnesium halide[7] (Y = M^2 = MgBr), and the resulting organozinc intermediates can be trapped by one- or two-carbon electrophiles.

After considerable experimentation, we found that the addition of (*E*)- and (*Z*)-zincated hydrazones [M^1 = Zn(II)] to (*E*)- and (*Z*)-alkenylboronates[8] (Y = BOR_2) takes place with high stereoselectivity.[9] A proper choice of the nontransferable ligand on the zinc(II) atom, as well as careful control of the trapping conditions, allowed us to achieve up to 99% diastereoselectivity (*ds*) in the coupling of three components overall (Scheme 1, bottom).

We now present a full account of the diastereoselective carbometalation of zincated hydrazones to alkenylboronates, stereoselective trapping of the resulting zinc/boron organodimetals, including the construction of the fourth stereogenic center derived from the electrophile, and application of an optically active hydrazone for the asymmetric construction of multiple stereogenic centers. Density functional theory (DFT) studies of the pathways of the addition reaction indicated a six-centered boat transition state, which accounts for the sense and degree of the diastereoselectivity.

Results and Discussion

Experimental Studies of the Feasibility and Stereoselectivity of the Reaction. The procedure for sequential three-component coupling of zincated hydrazones, alkenylboronates, and electrophiles is outlined in Scheme 2. Treatment of a starting hydrazone **A** with 2 equiv of *tert*-butyllithium[10] (*t*-BuLi; 1 equiv for deprotonation and 1 equiv as a ligand on the zinc atom) followed by addition of 1 equiv of anhydrous zinc chloride in ether produces a zincated hydrazone **B**.[11] Solvent is removed in vacuo, and then an (*E*)- or (*Z*)-alkenylboronate **C** and hexane are added. It should be noted that the addition reaction was much slower without removal of the ether.[12] The zincated hydrazone **B** adds to the (*E*)- or (*Z*)-alkenylboronate **C** at 0 °C for 12−48 h to give a B/Zn dimetallic species **D**, which upon electrophilic trapping gives a γ-borylhydrazone **E** in good to high overall yield. To achieve the excellent *ds*, a careful choice of workup conditions is mandatory, as hydrolysis of the hydrazone moiety under strongly acidic workup often resulted in 5−15% epimerization of the α-carbon center. Therefore, we hydrolyzed the γ-borylhydrazone **E** with aqueous propionic acid to minimize the epimerization (1−3% in most cases).

Effect of a Dummy Ligand on the Reactivity and *ds* of the Zincated Hydrazone. We first examined the reaction between hexenylboronates (**3*E*** and **3*Z***) and the *N*,*N*-dimethylhydrazone of 3-pentanone to investigate the effect of a nontransferable dummy ligand (R) on the zinc atom (Scheme 3). Each of the zincated hydrazones **2a**−**2c** was prepared by sequential treatment with *t*-BuLi (1 equiv), anhydrous $ZnCl_2$ (1 equiv), and the corresponding alkyllithium (1 equiv). The nature of the dummy ligand showed a significant impact on both the stereoselectivity and the reaction rate (Table 1). The reaction of zincated hydrazone **2a** bearing a *tert*-butyl ligand with (*E*)-hexenylboronate **3*E*** gave what we call here the *syn* adduct $\mathbf{4}_{\mathbf{syn}}$ in excess (95.2:4.8) of the alternative *anti* adduct in 88% yield (entry 1). On the other hand, the reactions of **2b** and **2c** with (*E*)-hexenylboronate **3*E*** gave the *anti* adduct $\mathbf{4}_{\mathbf{anti}}$ as the major diastereomer (45.0:55.0 and 32.9:67.1, respectively) in moderate

(6) Kubota, K.; Nakamura, E. *Angew. Chem., Int. Ed. Engl.* **1997**, *36*, 2491–2493.
(7) Nakamura, E.; Kubota, K.; Sakata, G. *J. Am. Chem. Soc.* **1997**, *119*, 5457–5458.
(8) (a) Nakamura, M.; Hara, K.; Hatakeyama, T.; Nakamura, E. *Org. Lett.* **2001**, *3*, 3137–3140. (b) Cooke, M. P., Jr. *J. Org. Chem.* **1994**, *59*, 2930–2931. (c) Cooke, M. P., Jr.; Widener, R. K. *J. Am. Chem. Soc.* **1987**, *109*, 931–933.
(9) Preliminary communication: (a) Nakamura, M.; Hatakeyama, T.; Hara, K.; Fukudome, H.; Nakamura, E. *J. Am. Chem. Soc.* **2004**, *126*, 14344–14345.
(10) When we used LDA in THF for deprotonation, the subsequent addition reaction was very slow. We assume that the diisopropylamine or THF slowed down the addition reaction through coordination to the zinc atom.
(11) The X-ray structure of the lithiated hydrazone has been reported (*s-trans*, as in **SM6** in Figure 8). See: Collum, D. B.; Kahne, D.; Gut, S. A.; Depue, R. T.; Mohamadi, F.; Wanat, R. A.; Clardy, J.; Duyne, G. V. *J. Am. Chem. Soc.* **1984**, *106*, 4865–4869.
(12) The rate of the addition reaction increased in the order THF < Et_2O < hexane. We assume that coordinative solvents prevent π-complex formation between the zincated hydrazone and alkenylboronates, such as in **CP3** and **CP4** in Figure 8.

Table 2. Diastereoselective Addition of Zincated Hydrazones to (*E*)- or (*Z*)-Alkenylboronates

entry[a]	zincated hydrazone[b,c]	alkenylboronate[d]	major diastereomer yield[e], *syn*:*anti*[f]
1	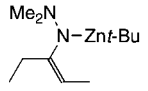 **2a**	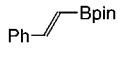 **5*E***: R = Ph 99.8% *E*	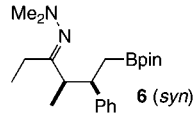 **6** (*syn*) 92%[g], 97.5:2.5
2	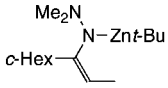 **7**	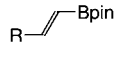 **8*E***: R = Me 99.3% *E*	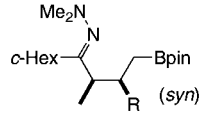 **10**: 93%, 99.2:0.8
3	**7**	**9*E***: R = Hex 99.5% *E*	**11**: 87%, 99.5:0.5
4	**7**	**5*E***: R = Ph 99.6% *E*	**12**: 80%, 99.6:0.4
5	**7**	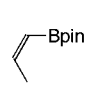 **8*Z*** 99.1% *Z*	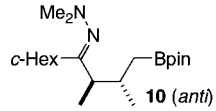 **10** (*anti*) 86%, 18.0:82.0
6	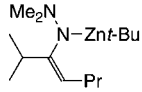 **13**	**8*E*** 99.3% *E*	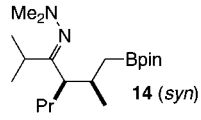 **14** (*syn*) 78%, 99.2:0.8
7	**13**	**8*Z*** 99.1% *Z*	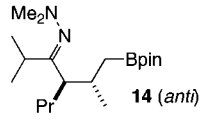 **14** (*anti*) 80%, 7.5:92.5
8	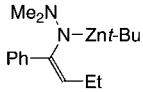 **15**	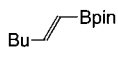 **3*E*** 99.7% *E*	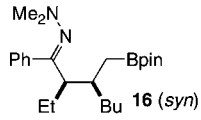 **16** (*syn*) 82%, 98.0:2.0
9	**15**	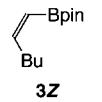 **3*Z*** 99.4% *Z*	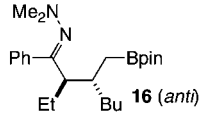 **16** (*anti*) 79%, 4.8:95.2

[a] Addition reactions were carried out in hexane at 0 °C for 12−48 h. [b] Zincated hydrazones **2a**, **7**, and **13** were prepared as in Scheme 2, and zincated hydrazone **15** was prepared as in Scheme 3. [c] The reactions used 1.05 equiv of **2a** or **7** or 1.25 equiv of **13** or **15**. [d] Bpin = 4,4,5,5-tetramethyl-1,3,2-dioxaborolanyl. [e] Isolated yield. [f] Diastereoselectivities were determined by GC analyses of the crude product. [g] Yield was determined by ^{1}H NMR spectroscopy.

yields (entries 2 and 3). Without any alkyl dummy ligand (i.e., ligand = Cl), the reaction did not take place at all (entry 4). As shown in entries 5−7, the reactions of **2a**−**2c** with (*Z*)-hexenylboronate **3*Z*** proceeded smoothly to give the *anti* adduct $\mathbf{4}_{\mathbf{anti}}$ as the major diastereomer. The zincated hydrazone **2a** showed slightly higher *ds* (25.6:74.4) than **2b** and **2c** (33.8:66.2 and 28.0:72.0, respectively). The relative stereochemistry of **4** was determined by X-ray and NMR analyses of the isolated compounds, as described in the Supporting Information (the stereochemical assignment of other products in Tables 2−4 is also described). We found that the *N*-alkyl- and *N*-arylimines used in our earlier studies[13] are less effective in the present reaction. We consider the zincated acyclic hydrazone **2** to be a (*Z*)-isomer in light of the stereochemistry of the addition of the zincated cyclic hydrazones, which is discussed later (see Theoretical Studies).

Table 3. Stereoselective Addition of Cyclic Substrates

entry[a]	zincated hydrazone[b,c]	alkenylboronate	major diastereomer yield[d], *syn*:*anti*
1	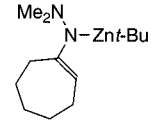 **17**	**8*E*** 99.3% *E*	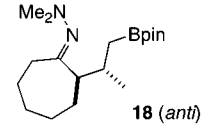 **18** (*anti*) 48%, 19.0:81.0[e]
2	**17**	**8*Z*** 99.1% *Z*	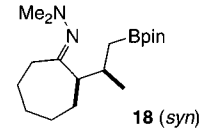 **18** (*syn*) 75%, 98.5:1.5[e]
3	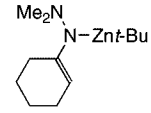 **19**	**8*Z*** 99.1% *Z*	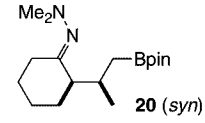 **20** (*syn*) 71%, 90:10[f]
4	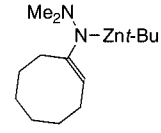 **21**	**8*Z*** 99.1% *Z*	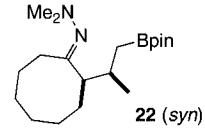 **22** (*syn*) 78%, 99.5:0.5[e]

[a] Addition reactions were carried out in hexane at room temperature (entry 1) or 0 °C (entries 2−4) for 48 h. [b] Zincated hydrazones **17**, **19**, and **21** were prepared as in Scheme 2. [c] The reactions used 1.25 equiv of **17**, **19**, or **21**. [d] Isolated yield. [e] Diastereoselectivity was determined by GC analyses of the crude product. [f] Diastereoselectivity was determined from the ^{1}H NMR spectrum of the crude product.

Diastereoselective Addition of Zincated Hydrazones to Alkenylboronates. Having established the conditions for the highly diastereoselective addition of zincated hydrazone **2a**, we studied the substrate scope on both the alkenylboronates and hydrazone substrates. Table 2 summarizes the results of the addition reactions of various acyclic zincated hydrazones with alkenylboronates. The reaction of **2a** with (*E*)-styrylboronate **5*E*** [99.6% (*E*)] gave *syn* adduct $\mathbf{6}_{\mathbf{syn}}$ in 92% yield with 97.5% *ds* (entry 1). Zincated hydrazone **7** prepared from 1-cyclohexylpropan-1-one *N*,*N*-hydrazone reacted with (*E*)-propenylboronate **8*E*** [99.3% (*E*)] to give *syn* adduct $\mathbf{10}_{\mathbf{syn}}$, which possesses two stereogenic centers, in 93% yield with 99.2% *ds* (entry 2). Also, the reactions of **7** with (*E*)-octenylboronate **9*E*** and (*E*)-styrylboronate **5*E*** proceeded with 99.5 and 99.6% *ds*, respectively (entries 3 and 4). The reaction of **7** with (*Z*)-propenylboronate **8*Z*** [99.1% (*Z*)] gave an alternative *anti* diastereomer $\mathbf{10}_{\mathbf{anti}}$ as the major product (82% *ds*, entry 5). Zincated hydrazone **13** prepared from 2-methylheptan-3-one reacted with **8*E*** and **8*Z*** to give adducts $\mathbf{14}_{\mathbf{syn}}$ (99.2% *ds*) and $\mathbf{14}_{\mathbf{anti}}$ (92.5% *ds*), respectively (entries 6 and 7). The reactions of zincated

(13) (a) Nakamura, M.; Hatakeyama, T.; Nakamura, E. *J. Am. Chem. Soc.* **2004**, *126*, 11820–11825. (b) Nakamura, M.; Hatakeyama, T.; Hara, K.; Nakamura, E. *J. Am. Chem. Soc.* **2003**, *125*, 6362–6363.

Table 4. Stereoselective Synthesis of γ-Boryl Hydrazones **E** via the Addition/Trapping Sequence

entry[a]	ZnHyd[b,c]	alkenyl-boronate[d]	electro-phile[e]	major diastereomer solvent[f], yield[g], *ds*[h]
1	**7**			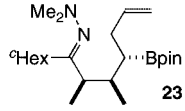 **23**
		8*E* 99.3% *E*		Et_2O: 86%, **99.2**:0.1:0.5:0.2 THF: 89%[i], 71.5:27.8:0.6:0.1
2	**13**	**8*E***		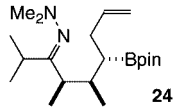 **24**
				86%, **> 99% *ds***[j]
3	**17**			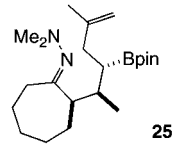 **25**
		8*Z* 99.1% *Z*		Et_2O: 70%, **94.7**:3.5:1.7:0.1 THF: 72%[i], 80.3:17.7:1.9:0.1
4	**15**	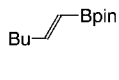		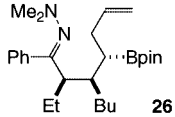 **26**
		3*E* 99.7% *E*		Et_2O: 80%, **97.6**:1.0:1.0:0.4 THF: 82%[i], 59.8:38.5:1.5:0.2
5	**15**			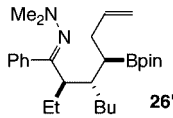 **26'**
		3*Z* 99.0% *Z*		Et_2O: 79%[i], 4.5:0.1:63.3:32.1 THF: 78%, 2.5:2.1:**83.0**:12.4
6	**7**	**8*E***		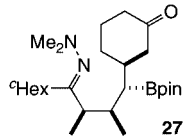 **27**
				69%, **> 95%*ds***[j]

[a] Addition reactions were carried out in hexane at 0 °C for 12−48 h. [b] Zincated hydrazones **7** and **17** were prepared as in Scheme 2, and zincated hydrazone **15** was prepared as in Scheme 3. [c] The reactions used 1.05 equiv of **7** or **13** or 1.25 equiv of **15** or **17**. [d] Bpin = 4,4,5,5-tetramethyl-1,3,2-dioxaborolanyl. [e] Electrophilic trapping was carried out in Et_2O with 1−2 equiv of CuCl and 2−4 equiv of electrophile. [f] Solvent in the trapping step. [g] Isolated yield. [h] Diastereoselectivities were determined by GC analyses of the crude product. [i] The yields were determined by ^{1}H NMR spectroscopy using pyridine as the internal standard. [j] This number refers to the percentage of the major isomer over all others as determined by ^{1}H NMR spectroscopy.

hydrazone **15** derived from an aryl alkyl ketone proceeded in a similar manner: the reactions with **3*E*** and **3*Z*** gave *syn* adduct $\mathbf{16}_{\mathbf{syn}}$ (98.0% *ds*) and *anti* adduct $\mathbf{16}_{\mathbf{anti}}$ (95.2% *ds*), respectively (entries 8 and 9).

Addition of Zincated Cyclic Hydrazones to Alkenylboronates. The reactions of cyclic hydrazone substrates and (*E*)- and (*Z*)-alkenylboronates are shown in Table 3. The reaction of cycloheptanone hydrazone **17** with (*E*)-propenylboronate **8*E*** gave *anti* adduct $\mathbf{18}_{\mathbf{anti}}$ with 81% *ds* at room temperature (entry 1). On the other hand, the reaction with (*Z*)-propenylboronate **8*Z*** was much faster (even at 0 °C) and gave the *syn* diastereomer $\mathbf{18}_{\mathbf{syn}}$ with 98.5% *ds* (entry 2). Six- and eight-membered-ring substrates **19** and **21** gave the corresponding products $\mathbf{20}_{\mathbf{syn}}$ and $\mathbf{22}_{\mathbf{syn}}$ with comparable chemical yields and selectivities (entries 3 and 4). The inversion of the *ds* between the acyclic (**2a**, **7**, **13**, and **15**) and cyclic (**17**, **19**, and **21**) hydrazones strongly suggests that the addition reactions of the acyclic hydrazones proceed from (*Z*)-isomers. The observed *ds* can be explained with the six-centered boat transition state (TS) model obtained from DFT calculations as described later.

Stereoselective Trapping of the Zn/B Organodimetals. When the addition of a zincated hydrazone to (*E*)- and (*Z*)-alkenylboronates is stereospecific and the stereogenic center bearing zinc and boron is configurationally stable, we should be able to create additional contiguous stereogenic centers by trapping the B/Zn intermediate **D** with a carbon electrophile, as shown in Scheme 4. The reaction of **7** and **8*E*** followed by treatment with allyl bromide (2.4 equiv) in the presence of CuCl (1 equiv) in Et_2O gave γ-borylhydrazone **23** in 86% yield with an overall *ds* of 99.2% (Table 4, entry 1). When THF was used as the solvent, the stereoselectivity dropped to 71.5% because of epimerization of the carbon center to which the Zn and B atoms are bonded. The stereochemistry of the third stereogenic center, along with the *syn*-addition nature of the first carbozincation, indicates that the electrophilic trapping occurred with overall retention of the stereochemistry of the B/Zn organodimetals (see below). This addition/trapping sequence starting from substrate **13** gave the corresponding adduct **24** with >99% *ds* (entry 2).[14]

The B/Zn intermediate **D** undergoes epimerization at the dimetalated stereogenic carbon center under these reaction conditions. The production of compounds possessing the same relative stereochemistry (i.e., **23** and **25**) starting from either (*E*)- or (*Z*)-alkenylboronate (entries 1 and 3) must be the consequence of such stereomutation of the dimetallic stereocenter. On the basis of the observed reduction in the *ds* in THF (entries 1, 3, and 4), we assume that the configuration of the B/Zn stereocenters is controlled by the conformation of the six-membered chelate structure of the product **D** (Figure 1).

Trapping of the B/Zn intermediate **D** produced by the reaction of **15** and **3*E*** gave adduct **26** possessing the same stereochemistry as **23**, **24**, and **25** (97.6% *ds*, entry 4). On the other hand, the reaction of **15** and **3*Z*** followed by trapping with allyl bromide in Et_2O gave mainly the other diastereomer **26′** with 63.3% *ds* (entry 5). As shown in Figure 1, the B/Zn intermediate **D** might favor the *anti* configuration at the β- and γ-carbons because of the conformational stability of the six-centered chelate structure, in which the boryl group and the substituent on the β-carbon of the *anti* configuration can occupy the less-hindered equatorial positions. Interestingly, trapping of the intermediate **D** prepared from **15** and **3*Z*** in THF gave the adduct **26′** with a better *ds* of 83.0%.

The three-component coupling protocol can create four stereogenic centers in a highly stereocontrolled fashion. Thus, the B/Zn intermediate **D** produced by the reaction of **7** and **8*E*** underwent 1,4-addition with 2-cyclohexen-1-one in the presence of Me_3SiCl[3] and CuCl to produce the three-component coupling product **27** in 69% overall yield with >95% overall *ds* (entry 6). We can understand the stereochemistry of the 1,4-addition in terms of the reported TS of the conjugate addition of an organocopper compound to cyclohexenone[15] (Figure 2).

(14) (a) Hupe, E.; Calaza, M. I.; Knochel, P. *Chem.—Eur. J.* **2003**, *9*, 2789–2796. (b) Boudier, A.; Knochel, P. *Tetrahedron Lett.* **1999**, *40*, 687–690.

Scheme 4. Stereocontrolled Trapping of the B/Zn Organodimetal **D** with Carbon Electrophiles

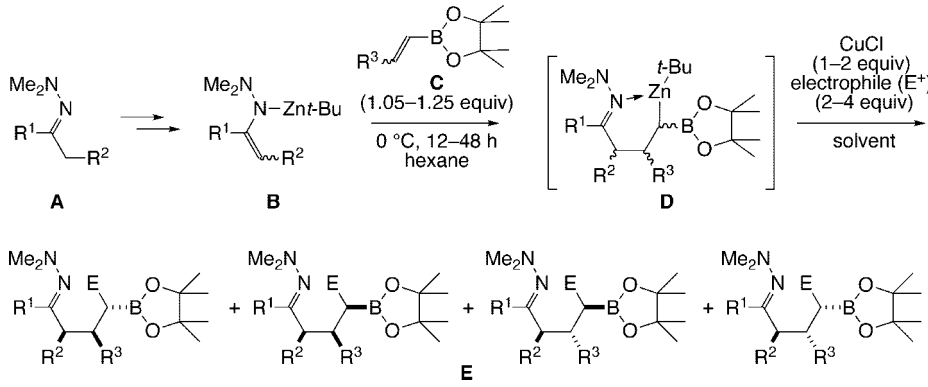

Asymmetric Construction of Three Contiguous Stereogenic Centers. We examined the asymmetric version of the three-component coupling using optically active (*S*)-1-amino-2-methoxymethylpyrrolidine (SAMP) hydrazone[16] **28**. The corresponding chiral zincated hydrazone **29** was prepared accordingly and allowed to react with **3*E*** at room temperature for 72 h. Successive trapping with allyl bromide gave adduct **30** in 63% yield with 95% overall *ds* (>99% *ds*, >99% *ee* after recrystallization) (eq 1). The stereochemistry of the product was

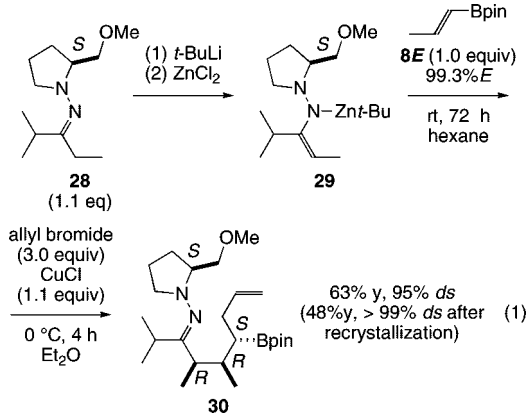

determined by X-ray crystallography. It is noteworthy that the absolute configuration of the α-carbon is opposite to that of the α-carbon in the products obtained by the alkylation reaction of lithiated SAMP hydrazones with alkyl halides.[17]

Hydrolysis of the Hydrazone and Oxidative Cleavage of the Bpin Group. γ-Borylhydrazones such as **25** can be used for further synthetic transformations in a stereoselective manner. Hydrolysis of the hydrazone moiety can be achieved readily (albeit with slightly less stereochemical control), and the ketone group can be reduced stereoselectively with BH_3·THF. The Bpin group was converted stereospecifically to a hydroxy group (the terminal double bond was hydrogenated before the reduction to avoid hydroboration). The diol **32** was obtained with 85% *ds*, with other minor diastereomers accounting for the rest. Esterification of the diol and recrystallization gave diester **33** with 99% *ds* (eq 2), and the stereochemistry was assigned by X-ray crystallography.

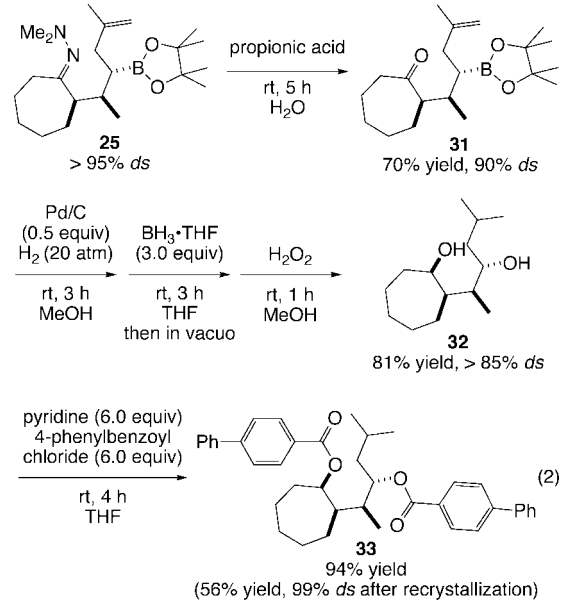

Theoretical Studies of the Addition of Zincated Hydrazones to Alkenylboronates. To gain mechanistic insights into the origin of the high diastereoselectivities, we conducted a series of theoretical/computational studies of the addition of zinc

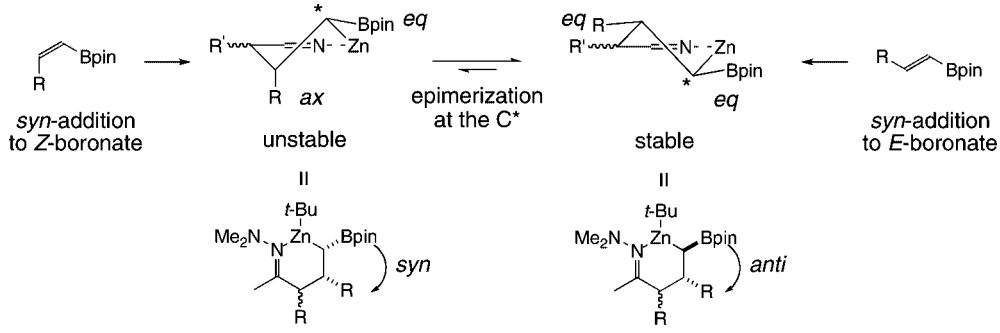

Figure 1. Conformational stability of the organozinc intermediate.

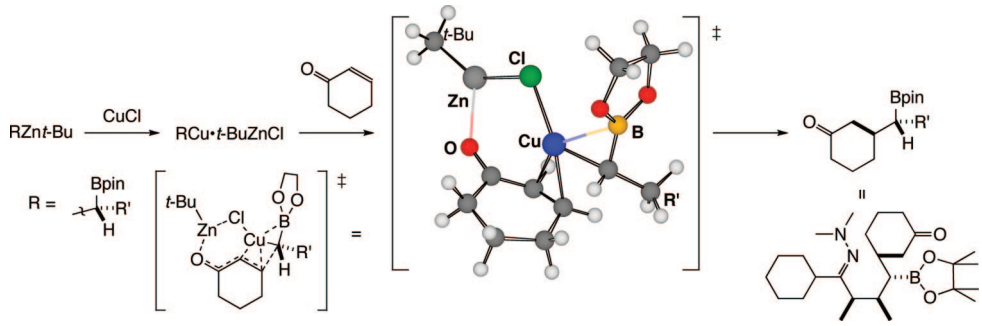

Figure 2. A possible transition structure for the 1,4-addition of B/Zn dimetallic species.

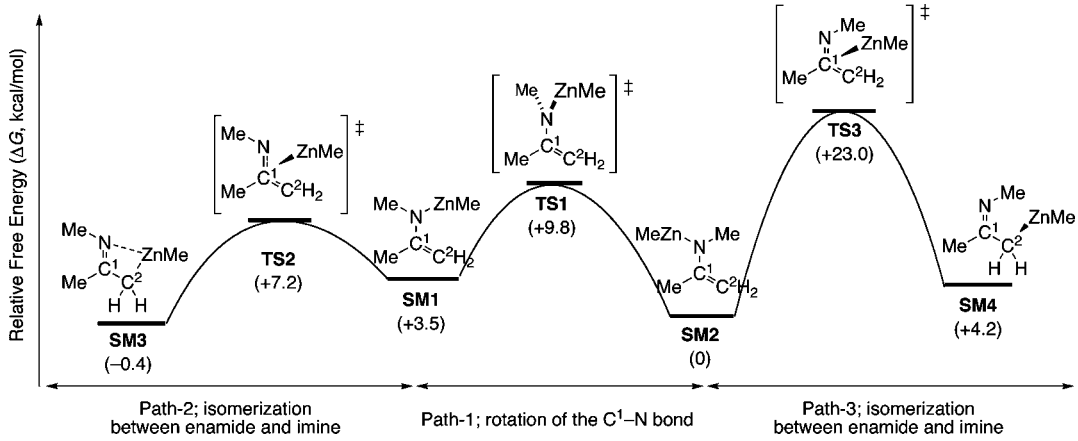

Figure 3. Energy profiles for the isomerization of the zinc enamides and their isomers. Relative free energies (Δ*G*, kcal/mol) with respect to **SM2** are shown in parentheses.

enamides and zincated hydrazones to alkenylboronates (or ethylene). Details of the theoretical methods are described in the Experimental Section. We first examined the structure of a zincated *N*-methylenamide of acetone and its addition to ethylene (eq 3) as a simplified model at the B3LYP/631A level.

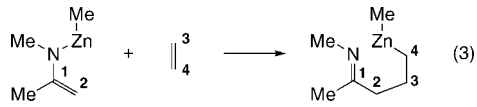

(3)

Structural Analysis of Zincated Imines. We found as stationary points four equilibrium structures arising from tautomerism and geometric isomerism of the C−N double bond: zinc enamides **SM1** and **SM2** and α-zincio imines **SM3** and **SM4**. **SM1** isomerizes to **SM2** via **TS1** (Figure 3, Path 1; numbers in parentheses represent free energies relative to **SM2**). **SM1** isomerizes to **SM3** via **TS2** (Path 2). **SM2** isomerizes to **SM4** via **TS3** (Path 3). These structures have free-energy differences of at most 23.4 kcal/mol.

The structures are shown in Figure 4. The zinc enamides **SM1** and **SM2** are conformational isomers with respect to rotation around the C^1-N bond. **SM1** is an *s-cis* conformer (C^2-C^1-N-Zn dihedral angle = 27.8°, C^2-Zn distance = 3.033 Å), and **SM2** is an *s-trans* conformer (C^2-C^1-N-Zn dihedral angle = 180.0°, C^2-Zn distance = 4.155 Å) that is 3.5 kcal/mol lower in free energy than **SM1**. The TS of the rotation **TS1** (C^2-C^1-N-Zn dihedral angle = 94.3°, C^2-Zn distance = 3.682 Å) lies 9.8 kcal/mol above **SM1**.

The α-metallo imines **SM3** and **SM4** are geometrical isomers with respect to the C^1-N double bond and interconvert with each other through **SM1** and **SM2**. In the (*E*)-isomer **SM3**, the nitrogen atom is coordinated to the zinc atom (N−Zn distance = 2.398 Å). In **SM4**, which is 4.6 kcal/mol higher in free energy, there is no such coordination, and the C−Zn bond is perpendicular to the imine plane, as previously found in the crystal structure of a dimeric Reformatsky reagent.[18] **TS2**, the TS separating **SM3** and **SM1**, has an aza-π-allyl zinc structure, in which the N−Zn (1.976 Å) and C^1-Zn (2.334 Å) bond lengths are intermediate between those of **SM1** and **SM3**; this is also true of **TS3** (N−Zn and C^1-Zn distances of 2.133 and 2.422 Å, respectively). The energy barriers separating **SM1**−**SM4** are low enough to suggest that all of them may also be in equilibrium with each other under the reaction conditions (hexane as solvent). However, we were able to locate reaction pathways for the addition to ethylene only for the zinc enamides **SM1** and **SM2**.

Addition of Acetone Imine to Ethylene. We located a single reaction pathway each for **SM1** and **SM2** that takes place via a metallo-ene-type [4 + 2] TS,[19] as shown in Figures 5 and 6, respectively (Paths A and B). The mechanism is similar to the one discussed in the aldol reaction except for the important point that the boat TS (Path A) is favored over the half-chair TS (Path B). In both paths, the zinc enamide and ethylene first form a π complex, which then goes through a metallo-ene-type TS on

(15) (a) Yamanaka, Y.; Nakamura, E. *Organometallics* **2001**, *20*, 5675–5681. (b) Nakamura, E.; Mori, S.; Morokuma, K. *J. Am. Chem. Soc.* **1997**, *119*, 4900–4910.
(16) (a) Job, A.; Janeck, C. F.; Bettray, W.; Peters, R.; Enders, D. *Tetrahedron* **2002**, *58*, 2253–2329. (b) Enders, D.; Wortmann, L.; Peters, R. *Acc. Chem. Res.* **2000**, *33*, 157–169.
(17) Enders, D. *Chem. Scr.* **1985**, *25*, 139–147.
(18) Dekker, J.; Budzelaar, P. H. M.; Boersma, J.; Van der Kerk, G. J. M.; Spek, A. J. *Organometallics* **1984**, *3*, 1403–1407.

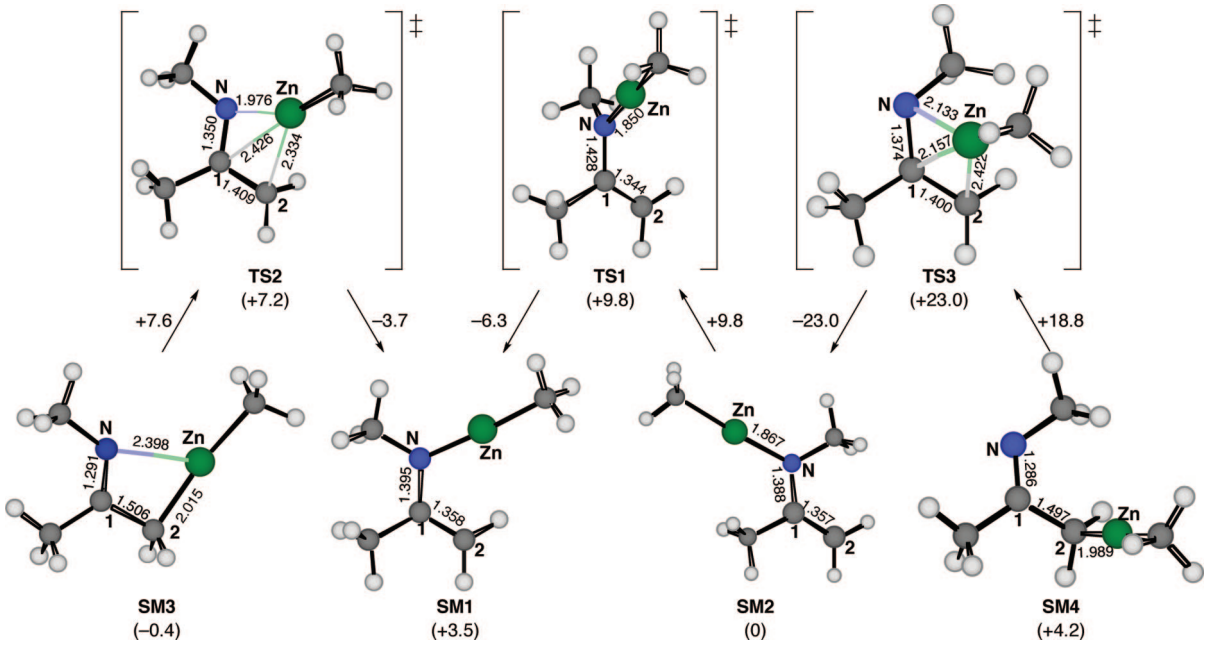

Figure 4. Isomerization pathway for the starting zinc enamide, as obtained from DFT calculations (B3LYP/631A). Free-energy changes (kcal/mol) and bond lengths (Å) are given. Relative free energies (ΔG, kcal/mol) with respect to **SM2** are shown in parentheses.

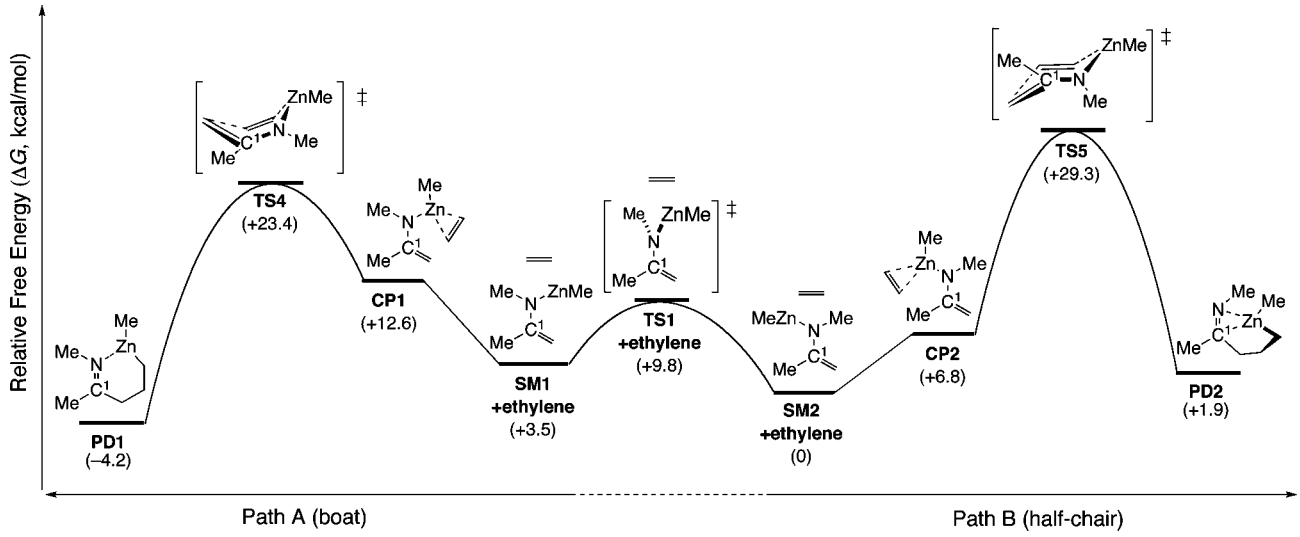

Figure 5. Energy profiles for the reaction pathways for addition of a zinc enamide to ethylene (B3LYP/631A). Relative free energies (ΔG, kcal/mol) with respect to **SM2** + ethylene are shown in parentheses.

its way to the product, in which zinc is covalently bonded in hand and coordinated to the imine group.

In Path A, **SM1** interacts with ethylene to form a π complex **CP1**, which is 9.1 kcal/mol higher in free energy than **SM1** + ethylene because of the entropy contribution.[20] The geometrical parameters indicate only a weak electrostatic interaction between the zinc center and the ethylene π electrons [N−Zn−Me angle = 169.2°, C^3−Zn distance = 3.178 Å, C^4−Zn distance = 3.078 Å, C^3−C^4 distance = 1.339 Å (compare to the C=C distance of 1.335 Å in ethylene)]. Formation of the C−C and C−Zn bonds in the next state takes place synchronously via **TS4** with a very low free energy of activation ($\Delta G^{\ddagger}$ = 10.8 kcal/mol) to form a nitrogen-chelated γ-zincio imine **PD1** with a stabilization energy of 27.6 kcal/mol.

TS4 is a six-centered boat transition state. The zinc enamide moiety still retains the original *s-cis* structure (C^2−C^1−N−Zn dihedral angle = 22.0°). The C^2−C^3 and C^4−Zn bond lengths indicate synchronous formation of these bonds, although the latter may be slightly more advanced. The imine in the product **PD1** is an (*E*)-imine, which was found in the product obtained after hydrolysis in the experiments (see above). The overall process of converting **SM1** and ethylene to **PD1** is exothermic (ΔG = −4.2 kcal/mol).

In Path B, **CP2** is 6.8 kcal/mol higher in free energy than **SM2** + ethylene.[21] The C−C and C−Zn bonds form via **TS5**,

(19) (a) Nakamura, M.; Hirai, A.; Nakamura, E. *J. Am. Chem. Soc.* **2000**, *122*, 11791–11798. (b) Hirai, A.; Nakamura, M.; Nakamura, E. *J. Am. Chem. Soc.* **1999**, *121*, 8665–8666. (c) Marek, I.; Schreiner, P. R.; Normant, J. F. *Org. Lett.* **1999**, *1*, 929–931. (d) Endo, K.; Hatakeyama, T.; Nakamura, M.; Nakamura, E. *J. Am. Chem. Soc.* **2007**, *129*, 5264–5271.

(20) **CP1** is 1.8 kcal/mol lower in total electronic energy than **SM1** + ethylene.

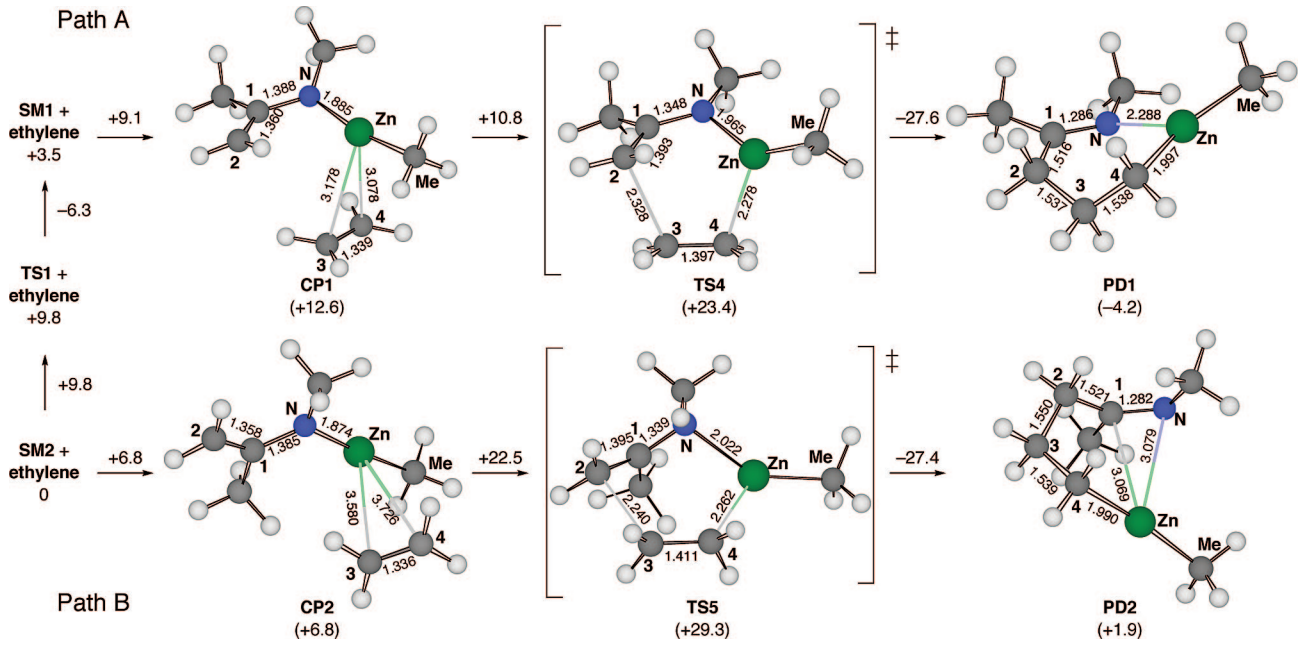

Figure 6. Reaction pathways for addition of a zinc enamide to ethylene, as obtained from DFT calculations (B3LYP/631A). Free-energy changes (kcal/mol) and bond lengths (Å) are given. Relative free energies (ΔG, kcal/mol) with respect to **SM2** + ethylene are shown in parentheses.

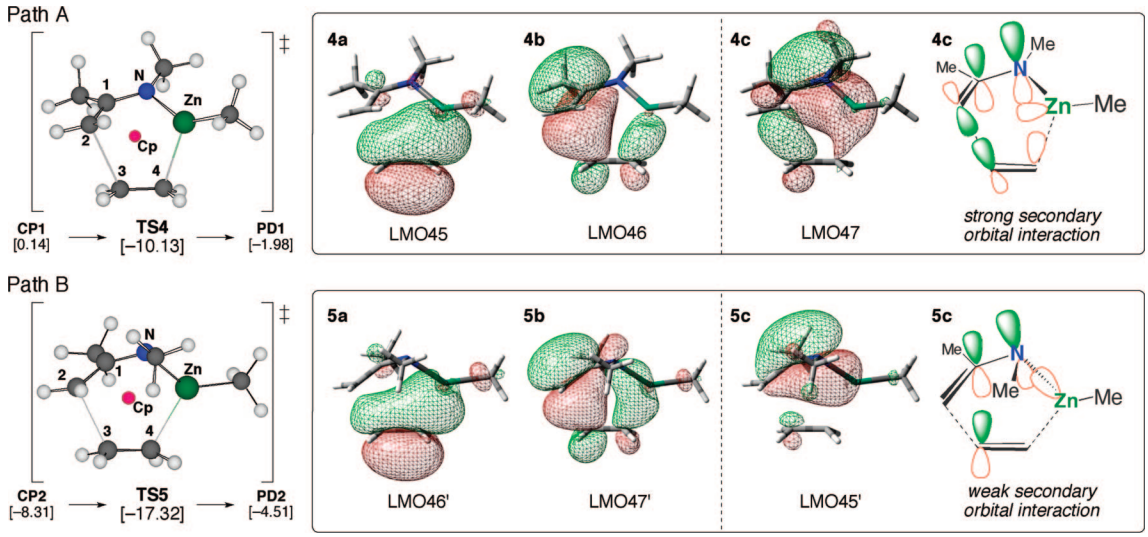

Figure 7. Natural localized molecular orbitals (NLMOs) of **TS4** (**4a**, LMO45; **4b**, LMO46; **4c**, LMO47) and **TS5** (**5a**, LMO46′; **5b**, LMO47′; **5c**, LMO45′). Nucleus-independent chemical shifts (NICS) values are shown in brackets at the left. Points labeled Cp are the center points of the [4 + 2] transition structures.

with a free energy of activation $\Delta G^{\ddagger} = 22.5$ kcal/mol, followed by formation of the γ-zincio imine **PD2** with a stabilization energy of 27.4 kcal/mol. **TS5** represents a half-chair conformer because of the *s-trans* conformation of the starting zinc enamide **SM2**. The C^2-C^1-N-Zn dihedral angle (106.0°) in **TS5** is larger than that in **TS4**, reflecting this conformation of **SM2**. The C^2-C^3 bond (2.240 Å) and the C^4-Zn bond (2.262 Å) are much shorter than those in **TS4**, indicating that **TS5** is reached later than **TS4**, which reflects the much higher free energy of activation for Path B than for Path A.

Path B produces a (*Z*)-imine, which does not agree with the experimental facts. In addition, the (*Z*)-geometry of the $C^1{=}N$ double bond forces the zinc atom to be π-coordinated to the $C^1{=}N$ double bond; as a result, the reaction is endothermic ($\Delta G = 1.9$ kcal/mol). Upon consideration of the whole scheme, **TS5** in Path B is 5.9 kcal/mol higher in free energy than **TS4** in Path A. We therefore conclude that the reaction takes place via Path A. The following analysis of the diastereoselectivities of the reactions is entirely consistent with this conclusion.

Two types of theoretical analysis were carried out to characterize the transition structures of the reaction: aromaticity analysis and orbital analysis. The aromaticity of the metalloene transition structures **TS4** and **TS5** was examined using GIAO calculations[22] at the B3LYP/631A level (Figure 7, left). Negative nucleus-independent chemical shift (NICS)[23] values (−10.13 and −17.32 for **TS4** and **TS5**, respectively) were

(21) **CP2** is 1.1 kcal/mol lower in total electronic energy than **SM2** + ethylene.

(22) Wolinski, K.; Hilton, J. F.; Pulay, P. J. *J. Am. Chem. Soc.* **1990**, *112*, 8251–8260.

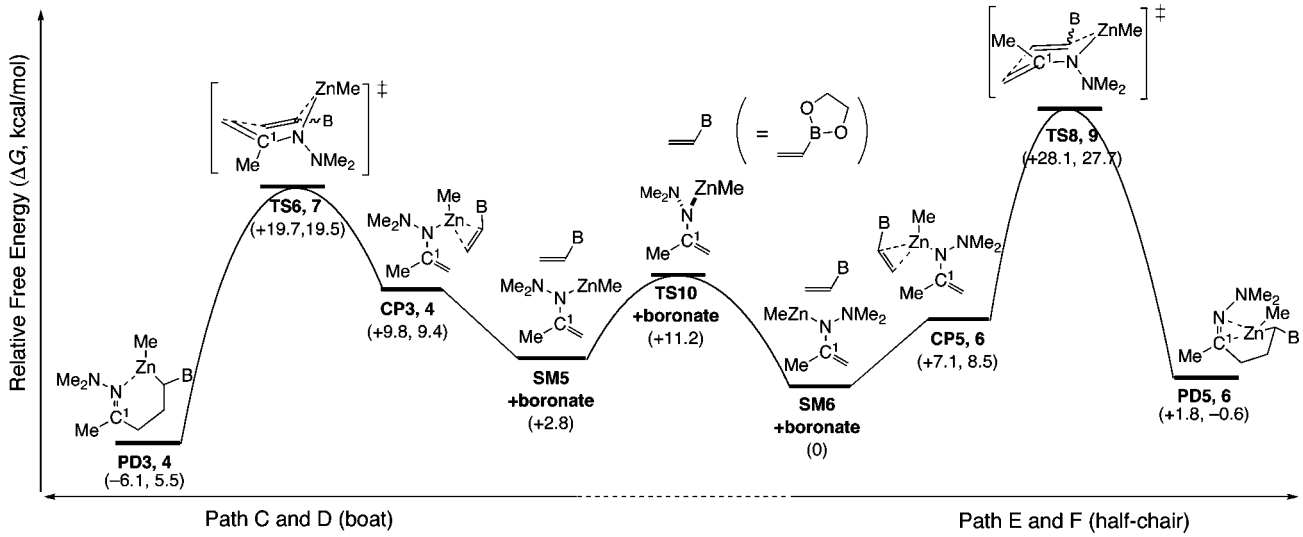

Figure 8. Reaction pathways for the addition of a zincated hydrazone to a vinylboronate, as obtained from DFT calculations (B3LYP/631A). Relative free energies (ΔG, kcal/mol) with respect to **SM6** + vinylboronate are shown in parentheses.

obtained at the center points (labeled as Cp in Figure 7) of the six heavy atoms included in the bond reorganization. These values are larger than those obtained likewise for the other stationary points on each reaction pathway (**CP1**, **CP2**, **PD1**, and **PD2**). This trend follows those found for pericyclic reactions in general, such as ene reactions,[23b] 1,3-dipolar cycloadditions,[24] and Diels−Alder reactions.[25]

Natural localized molecular orbital (NLMO) analysis[26] using the SCF Kohn−Sham orbitals of **TS4** and **TS5** provides insight into the molecular-orbital interactions between the zinc enamide and ethylene (Figure 7, right).[27] The in-phase orbital overlaps of the forming C−Zn and C−C bonds, respectively, are found in LMO45 (**4a**) and LMO46 (**4b**) for the boat **TS4** and in LMO46′ (**5a**) and LMO47′ (**5b**) for **TS5**. The LMOs **4a** and **5a**, consisting of the π orbital of ethylene and the zinc 4p orbital, are related to the C^4−Zn bond formation. The π^* orbital of ethylene and the π orbital of zinc enamide compose the LMOs **4b** and **5b**, which are responsible for the formation of the C^2−C^3 bond.

Whereas these orbital interactions are found equally in **TS4** and **TS5**, a striking difference is found in an in-phase secondary orbital interaction in LMO47 (**4c**), consisting of the nitrogen 2p orbital, the zinc 4s−4p hybrid orbital, and the forming C−C σ orbital. This orbital interaction is not found in **TS5**. Although the quantitative discussion of a secondary orbital interaction is always a matter of controversy, we think that this secondary orbital interaction in **TS4** may be a reason for the stability of **TS4** with respect to **TS5**.

Addition of Acetone Hydrazone to Vinylboronate. We next used the same B3LYP/631A theoretical model to examine a more realistic case: the addition of the enolate form of a zincated acetone hydrazone to a vinylboronate (eq 4). As in the enamide

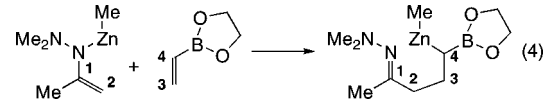
(4)

case, we located two types of pathway, one going through an energetically favorable boat TS (Paths C and D) and the other through an unfavorable half-chair TS (Paths E and F); in each case, the two paths involve diastereomers of similar energies arising because of the presence of the boryl group (Figure 8). The pathways involve the π complexes **CP3**−**CP6** and the six-centered TSs **TS6**−**TS9** and lead to the γ-zincio hydrazones **PD3**−**PD6**.

The two zincated hydrazones **SM5** (*s-cis*) and **SM6** (*s-trans*) are conformational isomers, separated from each other by **TS10**, the TS for rotation around the C^1−N bond ($\Delta G^{\ddagger} = 11.2$ kcal/mol, which is much smaller than the free energy of activation for the addition reaction, $\Delta G^{\ddagger} = 19.5$ kcal/mol). **SM5** and **SM6** each interact with the vinylboronate to form two diastereomeric π complexes (**CP3** and **CP4** from **SM5**, **CP5** and **CP6** from **SM6**).

Transition structures are shown in Figure 9. **TS6** and **TS7** are the boat conformers. The six-centered core structures resemble each other and **TS4** and **TS5** of the zincated enamide. The boryl group of **TS6** occupies an axial position and that of **TS7** an equatorial position, yet the free-energy difference in this simplest model is negligibly small ($\Delta G = 0.2$ kcal/mol).

TS8 and **TS9** are half-chair conformers. They are much less stable than **TS6** and **TS7** (by over 8.0 kcal/mol) and represent a later transition state, as was found previously for the zincated enamide counterparts. The lengths of the cleaving double bond C^3−C^4 (1.409 Å in **TS8** and 1.408 Å in **TS9** vs 1.390 Å in **TS6** and 1.389 Å in **TS7**) also suggest the advanced nature of **TS8** and **TS9**. The boryl group occupies an axial position in **TS8** and an equatorial position in **TS9**. **TS8** is less stable than **TS9** by only a small amount ($\Delta G = 0.4$ kcal/mol).

The products **PD3** and **PD4** have an (*E*) C^1=N double bond, in which the sp^2 nitrogen lone pair coordinates to the zinc atom.

(23) (a) Schleyer, P. v. R.; Maerker, C.; Dransfeld, A.; Jiao, H.; Hommes, N. J. R. v. E. *J. Am. Chem. Soc.* **1996**, *118*, 6317–6318. (b) Chen, Z.; Wannere, C. S.; Corminboeuf, C.; Puchta, R.; Schleyer, P. v. R. *Chem. Rev.* **2005**, *105*, 3842–3888.
(24) Cosśio, F. P.; Morao, I.; Jiao, H.; Schleyer, P. v. R. *J. Am. Chem. Soc.* **1999**, *121*, 6737–6746.
(25) Jiao, H.; Schleyer, P. v. R. *J. Phys. Org. Chem.* **1998**, *11*, 655–662.
(26) Reed, A. E.; Weinhold, F. *J. Chem. Phys.* **1995**, *83*, 1739–1740.
(27) For MO analyses of organozinc reactions using localized molecular orbital (LMO) and natural bond orbital (NBO) methods, see: (a) Mori, S.; Hirai, A.; Nakamura, M.; Nakamura, E. *Tetrahedron* **2000**, *56*, 2804. (b) Nakamura, E.; Yoshikai, N.; Yamanaka, M. *J. Am. Chem. Soc.* **2002**, *124*, 7181–7192. (c) Hratchian, H. P.; Chowdhury, S. K.; Gutiérrez-García, V. M.; Amarasinghe, K. K. D.; Heeg, M. J.; Schlegel, H. B.; Montgomery, J. *Organometallics* **2004**, *23*, 4636–4646.

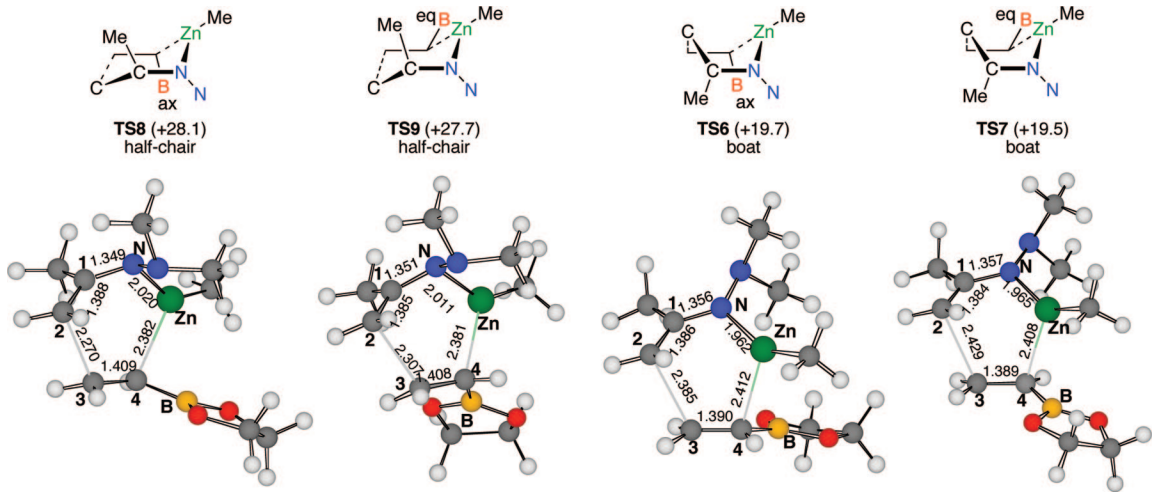

Figure 9. Transition structures **TS6**−**TS9** obtained from DFT calculations (B3LYP/631A). Relative free energies (Δ*G*, kcal/mol) with respect to **SM6** + vinylboronate are shown in parentheses. Bond lengths (Å) are also given.

In **PD5** and **PD6**, which possess a (*Z*) C^1═N double bond, the zinc atom is p-coordinated to the imine group. These products are less stable than **PD3** and **PD4** (Δ*G* = 4.9−7.9 kcal/mol). Detailed structural parameters for the stationary points are reported in the Supporting Information.

Analysis of Diastereoselectivity. With the conclusion that the boat transition state is overwhelmingly favored in the present reactions, we studied a series of additions of zincated hydrazones to (*E*)- and (*Z*)-propenylboronates via such boat transition states, to examine the origin of the high experimental diastereoselectivities.

We first studied three chemical models: the addition reactions of an (*E*)-propenylboronate with the zincated hydrazones derived from 3-pentanone *N*,*N*-dimethylhydrazone that possess methyl and *tert*-butyl groups on the zinc atom (denoted here as models 1 and 2, respectively) and with the one derived from 2-methyl-3-pentanone *N*,*N*-dimethylhydrazone that possesses a *tert*-butyl group on the zinc atom (denoted here as model 3). All of the diastereomeric transition structures of the boat conformation were fully optimized for these model reactions, and their relative electronic energies (Δ*E*) were compared.

Model 1 serves as a model for the addition to (*E*)-hexenylboronate of the zincated hydrazone derived from a 3-pentanone *N*,*N*-dimethylhydrazone that possesses a butyl group on the zinc atom (denoted here as exp-1), which gave the *anti* adduct as the major diastereomer (*syn*:*anti* = 32.9:67.1, as shown in entry 3 of Table 1). Model 2 serves as a model for the addition to (*E*)-hexenylboronate of the zincated hydrazone derived from a 3-pentanone *N*,*N*-dimethylhydrazone that possesses a *tert*-butyl group on the zinc atom (denoted here as exp-2), which gave the *syn* adduct as the major diastereomer (*syn*:*anti* = 95.2:4.8, as shown in entry 1 of Table 1). Model 3 serves as a model for the addition to (*E*)-propenylboronate of the zincated hydrazone derived from a 1-cyclohexylpropan-1-one *N*,*N*-dimethylhydrazone possessing a *tert*-butyl group on the zinc atom (denoted here as exp-3), which gave the *syn* adduct as the major diastereomer (*syn*:*anti* = 99.2:0.8, as shown in entry 2 of Table 2).

The calculations on models 1 and 2 were performed at the B3LYP/631A level, while calculations on models 2 and 3 were performed at the B3LYP/631A//2 L-ONIOM level. To check the results obtained by the B3LYP/631A//2 L-ONIOM method, we performed the calculations on model 2 using both methods and found that the relative energies are in very good agreement with each other. We also carried out polarizable continuum model (PCM) calculations on model 2 and found that the relative stabilities (Δ*E*) of each TS in the solvent (heptane) differ from those in the gas phase by less than 0.15 kcal/mol.[28] As shown in Figure 10, four isomeric transition structures of the boat conformation were obtained for each model (**TSA1**−**TSD1** for model 1, **TSA2**−**TSD2** for model 2, and **TSA3**−**TSD3** for model 3).

TSB1 is the most stable transition structure for model 1 and lies 0.16 kcal/mol lower in electronic energy (this Δ*E* corresponding to a *syn*:*anti* ratio of 42.7:57.3 at 273 K) than the second most stable structure (**TSD1**). The small energy difference agrees with the poor selectivity (*syn*:*anti* = 32.9:67.1) observed in exp-1. **TSA2** is the most stable transition structure for model 2. The second most stable structure (**TSC2**) is Δ*E* = 1.38 kcal/mol higher in electronic energy than **TSA2**. **TSB2** and **TSD2** are even higher in energy because of the steric repulsion between the *tert*-butyl group on the zinc atom and the pinacol moiety of the boryl group, which occupies an equatorial position. The relative energies (corresponding to a *syn*:*anti* ratio of 92.7:7.3 at 273 K) agree with the high diastereoselectivity obtained in the real system (*syn*:*anti* = 95.2:4.8).

For model 3, **TSA3** is the most stable, lying 3.64 kcal/mol lower in energy than the next most stable structure (**TSC3**). The low stability of **TSC3** is attributed to the additional steric repulsion between the isopropyl group and the methyl group on the enamide terminal. Accordingly, **TSB3** and **TSD3** are much higher in energy than **TSA3** and **TSC3** because of the steric repulsion between the isopropyl group and the methyl group on the boronate group. The relative electron energies (which yield a *syn*:*anti* ratio of 99.9:0.1 at 273 K) agree very well with the selectivity obtained in exp-3 (*syn*:*anti* = 99.2:0.8).

Overall, the computational results gave full support to the beneficial use of a *tert*-butyl group on the zinc atom and the effects of bulky substituents on the ketone skeleton. Such effects of the substituents on the metal and the substrates parallel the

(28) We used the heptane polarity for the PCM calculation. The relative energies of **TSA2**−**TSD2** obtained from the PCM calculation (B3LYP/631A) are 0, 2.37, 1.38, and 2.76 kcal/mol, respectively.

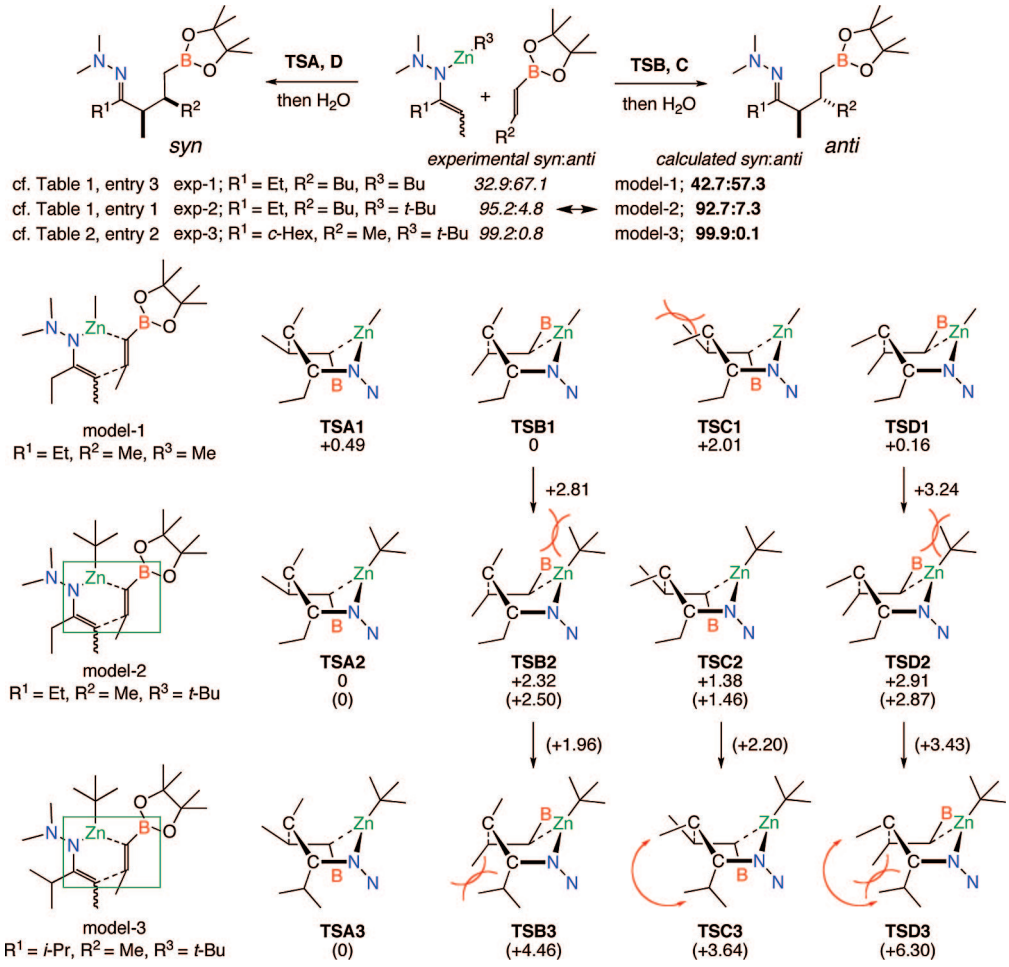

Figure 10. Transition structures for the addition of zincated hydrazones to an (*E*)-propenylboronate, as obtained from calculations at the B3LYP/631A and B3LYP/631A//2 L-ONIOM levels. Relative electronic energies (ΔE, kcal/mol) from the B3LYP/631A and B3LYP/631A//2 L-ONIOM methods are shown without and in parentheses, respectively. Diastereoselectivities calculated from the ΔE values at $T = 273$ K are shown in bold and those obtained experimentally in italics. The green squares in the model 2 and model 3 structures show the boundaries between the first and second layers used in the two-layered ONIOM calculations.

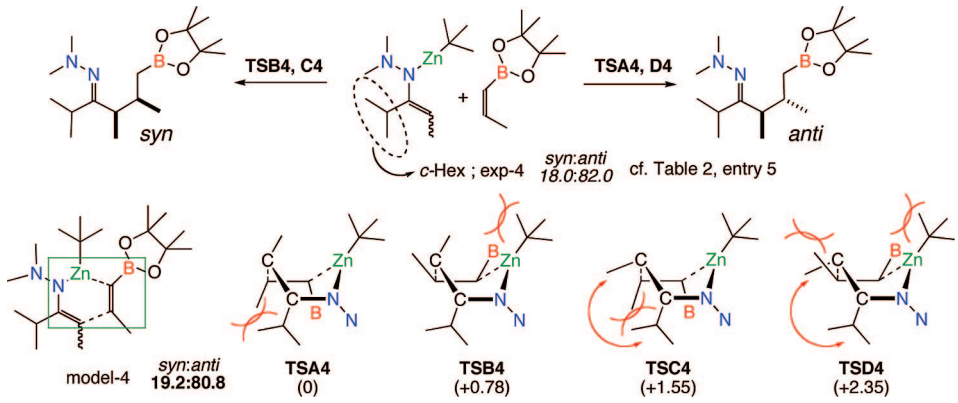

Figure 11. Transition structures for the addition of the zincated hydrazone derived from 2-methyl-3-pentanone to (*Z*)-propenylboronate, as obtained from calculations at the B3LYP/631A//2 L-ONIOM level. Relative electronic energies (ΔE, kcal/mol) are shown in parentheses. Diastereoselectivities calculated from the ΔE values at 273 K are shown in bold and those obtained experimentally in italics. The green square in the model 4 structure shows the boundary between the first and second layers used in the two-layered ONIOM calculations.

substituent effects known for the aldol reaction, except for the fundamental difference that the present reaction prefers boat transition states instead of chair transition states.

We then studied (at the B3LYP/631A//2 L-ONIOM level) the addition reaction between (*Z*)-propenylboronate and the zincated hydrazone derived from a 2-methyl-3-pentanone *N*,*N*-dimethylhydrazone possessing a *tert*-butyl group on the zinc atom (denoted here as model 4). Model 4 serves as a model for the addition to (*Z*)-propenylboronate of the zincated hydrazone derived from a 1-cyclohexylpropan-1-one *N*,*N*-dimethylhydrazone possessing a *tert*-butyl group on the zinc atom (denoted here as exp-4). As shown in Figure 11, the relative electronic

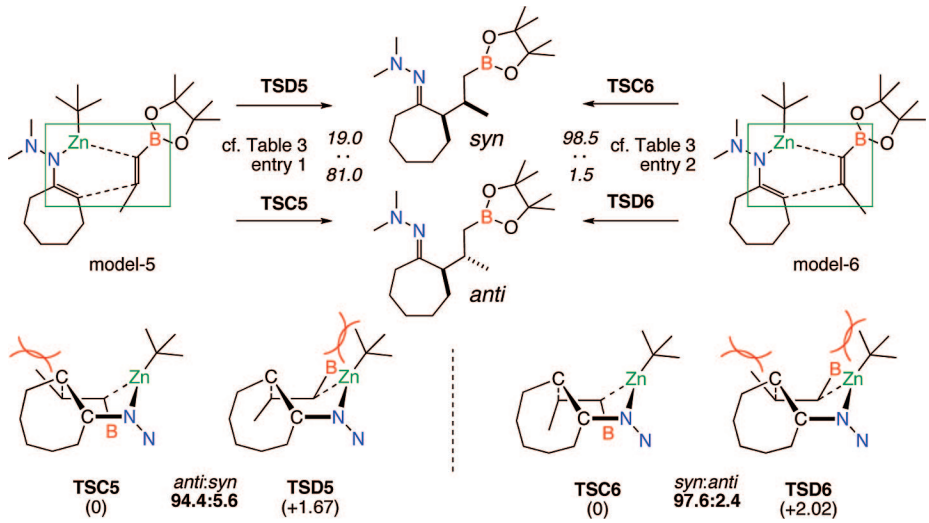

Figure 12. Transition structures for the addition of the zincated hydrazone derived from cycloheptanone to (*E*)- and (*Z*)-propenylboronate, as obtained from calculations at the B3LYP/631A//2 L-ONIOM level. Relative electronic energies (ΔE, kcal/mol) are shown in parentheses. Diastereoselectivities calculated from the ΔE values at 298 K for model 5 and 273 K for model 6 are shown in bold and those obtained experimentally in italics. The green squares in the models show the boundaries between the first and second layers used in the two-layered ONIOM calculations.

energies ΔE and corresponding calculated *syn*:*anti* ratios agree with the modest selectivity observed in exp-4 (*syn*:*anti* = 18.0:82.0, as shown in entry 5 of Table 2). The favored transition structure **TSA4** is only 0.78 kcal/mol lower in electronic energy than **TSB4** because of the steric repulsion between the isopropyl group and the methyl group on the boronate.

We also carried out B3LYP/631A//2 L-ONIOM calculations on the addition of the zincated hydrazone of cycloheptanone *N*,*N*-dimethylhydrazone to (*E*)- and (*Z*)-propenylboronate (models 5 and 6, respectively). Two transition structures were located for each model reaction (Figure 12). **TSD5** is 1.67 kcal/mol higher in electronic energy than **TSC5** because of the steric repulsion between the *tert*-butyl group and the pinacol moiety of the boryl group. **TSD6** is 2.02 kcal/mol higher in electronic energy than **TSC6** for the same reason. The larger energy difference between **TSC6** and **TSD6** than between **TSC5** and **TSD5** may be attributed to the steric repulsion between the methyl group on the boronate and the hydrazone side chain in **TSD5** and **TSC5**. The relative energies yield *syn*:*anti* ratios that agree well with the selectivities obtained experimentally (*syn*:*anti* = 19.0:81.0 for model 5 and *syn*:*anti* = 98.5:1.5 for model 6, as shown in entries 1 and 2, respectively, of Table 3).

The mechanistic studies showed that the high diastereoselectivity with respect to Cα atom and Cβ arises from the steric repulsion between the *tert*-butyl group on zinc and the pinacol moiety of the alkenylboronate in the six-centered boat transition structure. (*E*)- and (*Z*)-Alkenylboronates accordingly show the opposite selectivity. The cyclic zinc enamides (or zincated hydrazones) are by definition (*E*)-isomers, and the opposite selectivity observed for the acyclic substrates suggests that the acyclic zincated enamides are (*Z*)-isomers.

Conclusions

Zincated hydrazones possessing a *tert*-butyl dummy ligand on the zinc atom reacted with (*E*)- and (*Z*)-alkenylboronates with high diastereoselectivities in a stereospecific manner. The B/Zn organodimetallic intermediates produced by the aza-zincio-ene reaction were trapped in high yields by various carbon electrophiles in a stereoselective manner. The latter selectivity largely reflected the stereochemistry of the C−Zn bond in the intermediate. The carbometalation/trapping sequence achieved the three-component coupling of a zincated hydrazone, an alkenylboronate, and an electrophile, producing a γ-boryl hydrazone with contiguous stereogenic centers. The *ds* may exceed 99%. The γ-boryl hydrazones obtained by the multicomponent coupling are amenable to further synthetic elaborations, which would allow introduction of a variety of functional groups or additional stereogenic centers in a stereoselective fashion. In addition, the SAMP hydrazone shows a high level of asymmetric induction without loss of diastereomeric control in the addition/trapping sequence. We expect that the present method will be useful for the synthesis of optically active molecules possessing multiple stereogenic centers.

Through extensive computational and theoretical analyses, we have elucidated the reaction pathways of the present reaction; they feature the boat transition state as well as the origin of such a preference. Most importantly, the calculations indicated that the use of the zinc atom together with the imine or hydrazone has effectively lowered the activation energy and made the overall reaction exothermic and that this combination is the key to the success of the olefinic variant of the aldol reaction, which has long been considered not to take place because of the endothermicity of the reaction and has never been examined with any seriousness by chemists.

The high diastereoselectivity is the result of the mutual face selection between the nucleophilic sp^2 carbon and electrophilic sp^2 carbon dictated by the steric repulsion between the *tert*-butyl group on zinc and the pinacol moiety. Without any sterically hindered substituents, there would appear to be little selectivity. This is also true for the aldol reaction between a simple ketone enolate and a simple aldehyde. The mechanistic information described above will increase the reliability of the new synthetic strategy, which features stereocontrolled C−C bond formation by means of stereospecific olefin carbometalation reactions of metal enolates and their congeners.

Experimental Section

General. All of the reactions dealing with air- or moisture-sensitive compounds were carried out in a dry reaction vessel under a positive pressure of argon or nitrogen. Air- and moisture-sensitive

liquids and solutions were transferred via syringe or stainless-steel cannula. Analytical thin-layer chromatography was performed on glass plates coated with 0.25 mm, 230−400 mesh silica gel containing a fluorescent indicator (Merck, no. 1.05715.0009). Thin-layer chromatography plates were visualized by exposure to ultraviolet light (254 nm) and/or by immersion in an acidic staining solution of *p*-anisaldehyde followed by heating on a hot plate. Organic solutions were concentrated by rotary evaporation at ~30 mmHg. Flash column chromatography was performed on Kanto silica gel 60 (spherical, neutral, 140−325 mesh, pretreated with *N*,*N*-dimethylaniline for purification of hydrazones) as described by Still et al.[29]

Computational Methods. All of the calculations were performed with the Gaussian 03 package.[30] The DFT method was employed using the B3LYP hybrid functional.[31] Structures were optimized with a basis set (denoted here as 631A) consisting of Ahlrichs' SVP all-electron basis set[32] for the zinc atom and the 6-31G* basis set[33] for other atoms. In some reactions, geometry optimizations were performed using the two-layered ONIOM method (first layer, B3LYP/631A; second layer, HF/3-21G), and then energies were reevaluated by a single-point calculation with B3LYP/631A (this method is denoted here as B3LYP/631A//2 L-ONIOM). Each stationary point was adequately characterized by normal-coordinate analysis (no imaginary frequencies for an equilibrium structure and one imaginary frequency for a transition structure) using the same method as for the geometry optimization. Intrinsic reaction coordinate (IRC) analyses[34] were carried out throughout the reaction pathways using the same method as for the geometry optimization in order to confirm that all of the stationary points were smoothly connected to each other. NICS values were evaluated by using the gauge-invariant atomic orbital (GIAO) approach with B3LYP/631A (denoted here as GIAO-B3LYP/631A).

Instrumentation. Proton nuclear magnetic resonance (^{1}H NMR) and carbon nuclear magnetic resonance (^{13}C NMR) spectra were recorded with a JEOL AL-400 (400 MHz), JEOL ECX-400 (400 MHz), or JEOL ECA-500 (500 MHz) NMR spectrometer. Chemical-shift values (δ scale) for protons are reported in parts per million downfield from tetramethylsilane and are referenced to the residual proton of $CDCl_3$ (δ 7.26). ^{13}C NMR spectra were recorded at 125 or 100 MHz; chemical shifts for carbons (δ scale) are reported in parts per million downfield from tetramethylsilane and are referenced to the carbon resonance of $CDCl_3$ (δ 77.0). Data are presented as follows: chemical shift, multiplicity (s = singlet, d = doublet, t = triplet, q = quartet, quint = quintet, sext = sextet, sept = septet, m = multiplet and/or multiplet resonances, br = broad), coupling constant in hertz, signal area integration in natural numbers, and assignment (*italic*). IR spectra recorded on an FT/IR-420 (JASCO) or a React IR 1000 Reaction Analysis System equipped with DuraSample IR (ASI Applied System) are reported in cm^{-1}. Characteristic IR absorptions are reported except for normal aliphatic C−H absorptions (2980−2840 and 1470−1350 cm^{-1}). High-resolution mass spectra (HRMS) were obtained using the electron impact (EI) method with a JEOL GC-mate II instrument or the atmospheric pressure chemical ionization (APCI) or electrospray ionization (ESI) method with a JEOL JMS-T100LC instrument.

Solvents. Anhydrous diethyl ether (Et_2O) and hexane were purchased from Kanto Chemical Co. and degassed and dried over molecular sieves in a storage flask. The eluent for column chromatography (a 0:100 to 40:60 mixture of Et_2O and hexane) was dried over molecular sieves in a bottle. The water content of the solvent was confirmed with a Karl Fischer Moisture Titrator (MKC-210, Kyoto Electronics Company) to be less than 10 ppm. Anhydrous tetrahydrofuran (THF) was purchased from Kanto Chemical and distilled from benzophenone ketyl at 760 mmHg under argon immediately before use.

Materials. Unless otherwise noted, materials were purchased from Tokyo Kasei Kogyo Co., Aldrich Inc., and other commercial suppliers and were used after appropriate purification. $ZnCl_2$ (anhydrous, beads) was purchased from Aldrich. CuCl was purchased from Wako Co, and *t*-BuLi was purchased from Kanto Chemical and titrated before use. Florisil (100−200 mesh) was purchased from Yoneyama Yakuhin Kogyo Co., Ltd.

Typical Procedure for an Addition Reaction (Procedure A): (2*R,3*R**)-1-Cyclohexyl-2,3-dimethyl-4-(4,4,5,5-tetramethyl-1,3,2-dioxaborolan-2-yl)-1-butanone *N*,*N*-Dimethylhydrazone (10_{syn}).** *t*-BuLi (1.59 M in pentane, 1.26 mL, 2.0 mmol) was slowly added to a solution of the *N*,*N*-dimethylhydrazone of 1-cyclohexylpropan-1-one (0.182 g, 1.0 mmol) in hexane (1.0 mL) at −78 °C. The mixture was stirred at 0 °C for 1.5 h, and then $ZnCl_2$ (0.5 M in Et_2O, 2.0 mL, 1.0 mmol) was added at that temperature. After 15 min, the solvents were removed in vacuo (10 min, 0 °C, 0.1 mmHg). (*E*)-Propenylboronate **8*E*** [0.160 g, 0.95 mmol, 99.3% (*E*)] and hexane (0.4 mL) were slowly added at 0 °C. After 12 h, saturated aqueous $NaHCO_3$ (4.0 mL) was added at 0 °C. The aqueous layer was extracted with hexane (twice) and Et_2O (twice). The combined organic extracts were filtrated with a pad of Florisil using Et_2O as an eluent, and the *ds* (99.2%) was determined by GC analysis. The solvents were removed in vacuo, and the resulting crude product was purified by column chromatography on silica gel (15, 30% Et_2O in hexane) to give the title compound (0.309 g, 93% yield) as a colorless oil. R_f = 0.39 (20% AcOEt in hexane). IR (neat): 2813, 2769, 1625 (C=N), 1314, 1144, 959, 847. ^{1}H NMR: δ 0.64 (dd, J = 9.8, 15.5 Hz, 1H, C*H*HB), 0.87 (d, J = 7.0 Hz, 3H, CH(C*H*$_3$)CH$_2$B), 1.03 (d, J = 7.0 Hz, 3H, CCHC*H*$_3$), 1.06 (dd, J = 2.3, 15.5 Hz, 1H, CH*H*B), 1.15−1.20 (m, 1H, CH(CH$_2$)$_2$C*H*H), 1.25 (s, 12H, C(C*H*$_3$)$_2$C(C*H*$_3$)$_2$), 1.31−1.40 (m, 4H, (C*H*H)$_2$CH$_2$-(C*H*H)$_2$), 1.51−1.58 (m, 2H, CH*H*(CH$_2$)$_3$CH*H*), 1.67−1.76 (m, 3H, CH$_2$(CH*H*)$_3$CH$_2$), 1.99−2.03 (m, 1H, C*H*CH$_2$B), 2.12 (dq, J = 7.0, 9.0 Hz, 1H, CC*H*CH$_3$), 2.37 (s, 6H, N(C*H*$_3$)$_2$), 3.27 (tt, J = 3.0, 11.5 Hz, 1H, (CH$_2$)$_2$C*H*). ^{13}C NMR: δ 19.2, 21.3, 24.7 (2C), 24.9 (2C), 26.1, 26.1, 26.2, 29.2, 29.8, 33.7, 39.8, 42.5, 47.9 (2C), 82.7 (2C), 178.6. The NMR signal of the carbon α to the boron was not found. APCI-HRMS: calcd for $C_{20}H_{40}BN_2O_2$ $[M + H]^+$, 351.31865; found, 351.31917.

Typical Procedure for the Addition/Trapping Sequence: (2*R,3*R**,4*S**)-1-Cyclohexyl-2,3-dimethyl-4-[(3*S**)-3-oxocyclohexyl]-4-(4,4,5,5-tetramethyl-1,3,2-dioxaborolan-2-yl)butan-1-one *N*,*N*-Dimethylhydrazone (27).** The addition reaction was carried out according to procedure A on a 2.0 mmol scale. The solvents were removed in vacuo, and then Et_2O (1.0 mL) was added. The mixture of 2-cyclohexen-1-one (0.78 mL, 8.0 mmol), Me_3SiCl (1.02 mL, 8.0 mmol), and CuCl (0.396 g, 4.0 mmol) was added via a cannula at 0 °C. After 2 h, the reaction mixture was warmed to 20 °C and stirred for 2 h. Saturated aqueous $NaHCO_3$ (12 mL) and 10% aqueous ammonia (12 mL) were added at 0 °C. After the copper salts had dissolved, the aqueous layer was extracted with Et_2O (five times). The combined organic extracts were washed with brine, dried over anhydrous Na_2SO_4, and then filtered. The solvents were removed in vacuo, and the resulting crude product was purified by column chromatography on silica gel (20, 40% Et_2O in hexane) to give the title compound (0.555 g, 69% yield, >95% *ds* as determined by ^{1}H NMR spectra) as a white solid. Recrystallization from pentane gave crystals suitable for X-ray diffraction (>99% *ds*). R_f = 0.13 (20% AcOEt in hexane). IR (neat): 2814, 2768, 1714

(29) Still, W. C.; Klahn, M.; Mitra, A. *J. Org. Chem.* **1978**, *43*, 2923–2924.
(30) Frisch, M. J.; et al. *Gaussian 03*, revision C.02; Gaussian, Inc.: Pittsburgh, PA, 2003.
(31) (a) Becke, A. D. *J. Chem. Phys.* **1993**, *98*, 5648–5652. (b) Lee, C.; Yang, W.; Parr, R. G. *Phys. Rev. B* **1988**, *37*, 785–789.
(32) Schafer, A.; Horn, H.; Ahlrichs, R. *J. Chem. Phys.* **1992**, *97*, 2571–2577.
(33) Hehre, W. J.; Radom, L.; Schleyer, P. v. R.; Pople, J. A. *Ab Initio Molecular Orbital Theory*; John Wiley & Sons: New York, 1986. and references cited therein.
(34) (a) Fukui, K. *Acc. Chem. Res.* **1981**, *14*, 363–368. (b) Gonzalez, C.; Schlegel, H. B. *J. Chem. Phys.* **1989**, *90*, 2154–2161. (c) Gonzalez, C.; Schlegel, H. B. *J. Phys. Chem.* **1990**, *94*, 5523–5527.

(C═O), 1623 (C═N), 1311, 1144, 962, 846, 717. ^{1}H NMR: δ 0.80 (d, J = 6.8 Hz, 3H, CH(CH_3)CHB), 1.06−1.13 (m, 4H, CCHCH_3, $(CH_2)_2$CHH$(CH_2)_2$), 1.15−1.41 (m, 18H, (CHH)$_2$CH$_2$(CHH)$_2$, BCH, C$(CH_2)_2$CHH, C$(CH_3)_2$C$(CH_3)_2$), 1.51−1.63 (m, 3H, CH$H$$(CH_2)_3$-CH$H$, CCH_2CHH), 1.68−1.77 (m, 3H, CH_2(CHH)$_3$$CH_2$), 1.97−2.14 (m, 5H, C$H$(CH$_3$)CHB, C$H$HC(O)$CH_2$(CH$H$)$_2CH$), 2.18−2.27 (m, 2H, CC$HCH_3$, CC$HHCH_2$), 2.33−2.41 (m, 8H, CH$H$C(O)CH$H$, N(C$H_3$)$_2$), 3.40 (brt, J = 11.0 Hz, 1H, CH−$(CH_2)_5$−). ^{13}C NMR: δ 15.3, 20.0, 25.0 (2C), 25.1, 25.3 (2C), 25.7, 25.9, 26.2, 29.1, 29.8, 30.1, 33.0 (brs, α to the boron), 36.4, 38.1, 39.4, 39.9, 41.5, 47.8 (2C), 49.1, 83.0 (2C), 178.5, 211.8. Anal. Calcd for $C_{26}H_{47}BN_2O_3$: C, 69.94; H, 10.61; N, 6.27. Found: C, 69.95; H, 10.64; N, 6.17.

Acknowledgment. We thank the Ministry of Education, Culture, Sports, Science, and Technology of Japan for financial support and are grateful for a Grant-in-Aid for Scientific Research (S, E.N., 18105004), a Grant-in-Aid for Scientific Research on Priority Areas "Synergistic Effects for Creation of Functional Molecules" from MEXT (M.N., 18064006), and a Grant-in-Aid for Young Scientists from JSPS (T.H., 19750077).

Supporting Information Available: Experimental procedures, characterization data, and complete ref 30. This material is available free of charge via the Internet at http://pubs.acs.org.

JA806258V